Firefly Light Flashing: Oxygen Supply Mechanism

Article *in* Physical Review Letters · December 2014

DOI: 10.1103/PhysRevLett.113.258103 · Source: PubMed

10 authors, including:

Tzay-Ming Hong
National Tsing Hua University
90 PUBLICATIONS **665** CITATIONS

SEE PROFILE

Jen-Zon Ho
Endemic Species Research Institute
8 PUBLICATIONS **24** CITATIONS

SEE PROFILE

En-Cheng Yang
National Taiwan University
136 PUBLICATIONS **1,815** CITATIONS

SEE PROFILE

G. Margaritondo
École Polytechnique Fédérale de Lausanne
1,059 PUBLICATIONS **17,249** CITATIONS

SEE PROFILE

Firefly Light Flashing: Oxygen Supply Mechanism

Yueh-Lin Tsai,[1,2] Chia-Wei Li,[2,*] Tzay-Ming Hong,[3] Jen-Zon Ho,[4] En-Cheng Yang,[5] Wen-Yen Wu,[5] G. Margaritondo,[6] Su-Ting Hsu,[1] Edwin B. L. Ong,[1] and Y. Hwu[1,7,†]

[1]*Institute of Physics, Academia Sinica, Taipei 115, Taiwan*
[2]*Institute of Molecular and Cellular Biology, National Tsing Hua University, Hsinchu 300, Taiwan*
[3]*Department of Physics, National Tsing Hua University, Hsinchu 300, Taiwan*
[4]*Endemic Species Research Institute, Nantou 552, Taiwan*
[5]*Department of Entomology, National Taiwan University, Taipei 106, Taiwan*
[6]*Faculté des Sciences de Base, Ecole Polytechnique Fédérale de Lausanne (EPFL), CH-1015 Lausanne, Switzerland*
[7]*Advanced Optoelectronic Technology Center, National Cheng Kung University, Tainan 701, Taiwan*

(Received 28 July 2014; revised manuscript received 8 October 2014; published 17 December 2014)

Firefly luminescence is an intriguing phenomenon with potential technological applications, whose biochemistry background was only recently established. The physics side of this phenomenon, however, was still unclear, specifically as far as the oxygen supply mechanism for light flashing is concerned. This uncertainty is due to the complex microscopic structure of the tracheal system: without fully knowing its geometry, one cannot reliably test the proposed mechanisms. We solved this problem using synchrotron phase contrast microtomography and transmission x-ray microscopy, finding that the oxygen consumption corresponding to mitochondria functions exceeds the maximum rate of oxygen diffusion from the tracheal system to the photocytes. Furthermore, the flashing mechanism uses a large portion of this maximum rate. Thus, the flashing control requires passivation of the mitochondria functions, e.g., by nitric oxide, and switching of the oxygen supply from them to photoluminescence.

DOI: 10.1103/PhysRevLett.113.258103 PACS numbers: 87.18.Nq, 87.19.Wx, 87.59.-e, 87.85.Rs

Firefly flashing has fascinated humankind for millennia. It is now considered a possible biocommunication instrument [1–3], and has already led to applications [4–6]. The underlying biochemistry was recently clarified [7–11]. However, the physics side of the process, concerning the gas dynamics, is still unclear [1]. A leading model of the flashing control mechanism assumes that nitric oxide (NO) reduces the mitochondria activity, making available for bioluminescence a sufficient portion of the oxygen flux from the tracheal system. The supporting experimental evidence is the dense distribution of mitochondria organelles around the smallest trachea branches (tracheoles) [1,12–14] and the fact that NO stimulates luminescence whereas scavenger NO disables it. But these features cannot rule out an alternate hypothesis: the presence of the tracheole fluid could modulate the oxygen flux providing the extra amount for flashing [15,16].

Our study solves this dilemma in favor of the first hypothesis. We consistently reached this conclusion for two firefly types, *Luciola terminalis (L. terminalis) and Luciola cerata (L. cerata)*. We specifically used x-ray microscopy and tomography with spatial resolution < 20 nm to obtain a detailed three-dimensional mapping of the lantern, including the smallest branches ("tracheoles," diameter ~200 nm [17–20]) that are the most important for the gas exchange.

From the tracheole area and from Henry's law, we derived the total oxygen diffusion capacity assuming no fluid in the tracheoles [21]. We then evaluated the oxygen diffusion rates corresponding to mitochondria functions using the volume of the mitochondria zone adjacent to tracheoles, the mitochondrial protein density and the protein oxygen consumption. Finally, we evaluated the oxygen consumption for flashing from the emission of firefly lanterns, when stimulated by a pulsed current generator simulating neuronal signals.

The key quantitative results are for *L. terminalis*, a reasonable upper estimate of the oxygen diffusion is 21 p mol/s. This limit value can be stretched to 88.2 p mol/s only assuming an unrealistically large value of p, the oxygen partial pressure difference between tracheoles and photocytes. The oxygen consumption rate corresponding to mitochondrial functions is 127 p mol/s, and the consumption for flashing is 18.6 p mol/s. Thus, the oxygen flux is lower than the level required to entirely support mitochondria functions, and comparable to the flashing consumption. Therefore, flashing requires switching the oxygen supply from normal mitochondria activities to bioluminescence, as hypothesized by the NO model.

For *L. cerata*, the most reasonable upper value for the oxygen diffusion is 17.5 p mol/s (reaching 73.5 pmol/s for the extreme p value); the consumption rate for mitochondrial functions is 66.3 p mol/s, and that for flashing is 11.0 p mol/s. Thus, the conclusion is the same as for *L. terminalis*.

We would like to note an essential feature of our experiments. Advanced x-ray imaging was facilitated by the large refractive index differences at all interfaces

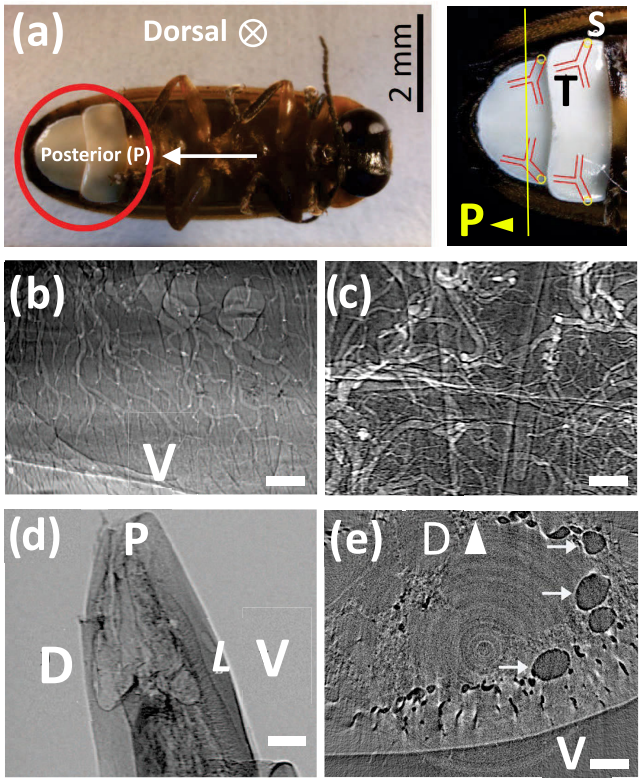

FIG. 1 (color online). (a) Pictures showing the lantern (white area) position and explaining the orientations of the x-ray images. Both images are ventral views. (b) and (c) Snapshots from an x-ray movie of the tracheal system in a live *L. terminalis* lantern. Scale bar: 200 μm. The detailed structures of the tracheal system can be clearly seen without any specimen processing. (d) Phase-contrast projection image showing the internal anatomy. Scale bar: 400 μm. (e) Typical tomographically reconstructed image showing a cross-sectional view of the abdomen of *L. terminalis*. The closed dark-gray circles correspond to the tracheae (arrows). Scale bar: 100 μm. D: Dorsal; V: Ventral; P: Posterior; L: Lantern; S: Spiracle openings; T: Tracheal system.

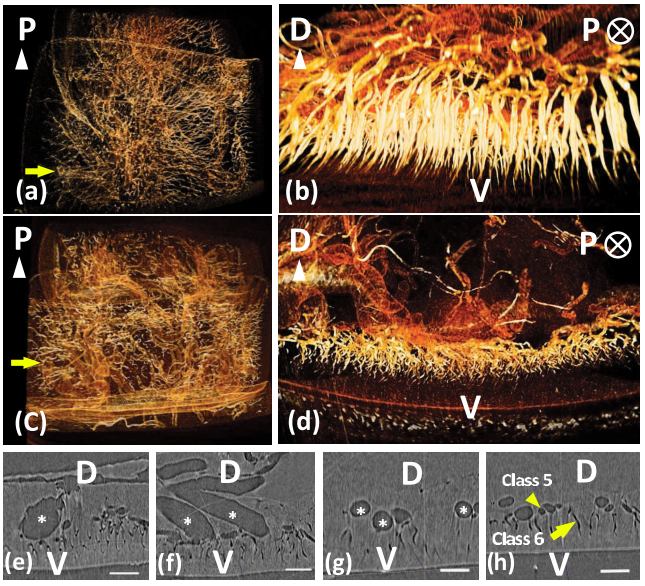

FIG. 2 (color online). Three-dimensional views of the tracheal system in *L. terminalis* (a)–(b) and *L. cerata* (c)–(d). (a) and (c): Dorsal views of reconstructed images taken with a 5 × objective (equivalent to a 3D volume of $1.6 \times 1.6 \times 1.2$ mm^3) show the ramifying tracheal anatomy from spiracles (arrows) to thin branches (the type 6 tracheae). (b),(d) Cross-sectional views of 3D pictures reconstructed from x-ray images taken with a 10 × objective ($0.8 \times 0.8 \times 0.6$ mm^3) reveal the details of type 6 tracheae with < 700 nm diameter. (e)–(h) X-ray tomography reconstructed cross-sectional images of type 1-6 tracheae. Type 4 tracheae are marked by asterisks, whereas a type 5 trachea is marked by an arrowhead and a type 6 trachea by an arrow. Scale bars: 100 μm.

between the tracheal system and air. This feature is ideal for phase contrast [22,23]. Figures 1(b) and 1(c) illustrate this point by showing single frame images from x-ray movies of the lantern of live fireflies. The tracheal system movements are clearly observed.

For quantitative evaluations, we used images obtained with phase-contrast microscopy and tomography like those of Figs. 1(d) and 1(e). We specifically reconstructed slices [e.g., Fig. 1(e)] from a single pixel line in the projection images [see Fig. 1(d), or, for example, the abdomen position marked by a yellow line in Fig. 1(a)]. Then, we combined the slices in three dimensions to show the entire tracheal system with a resolution similar to two-dimensional imaging. This enabled us to perform accurate measurements of structural parameters including trachea lengths and cross sections, by way of visual inspection and computer analysis.

The images revealed seven types of trachea branches with decreasing average diameters [Figs. 2(e)–2(i)], ranging from 120 μm [type 1, connected to exoskeleton spiracle openings, Figs. 2(a), 2(c), 2(e)] to < 300 nm (type 7 tracheoles). The resolution of in-line phase contrast imaging was not sufficient to detect the smallest structures, which required instead transmission x-ray microscopy (TXM) [24–26]. See, for example, the results of Fig. 3 that clearly reveal small branches, once again thanks to phase contrast.

The smallest branches, types 6 and 7, dominate the gas supply to photocytes. To estimate their total area (see the details in the Appendix), we measured the density of type 6 tracheae obtaining 349 $\pm$36 mm^{-2} (4 specimens) for *L. terminalis* and 466 ± 65 mm^{-2} (4 specimens) for *L. cerata*. The corresponding evaluated total lantern areas were 4.71 and 3.45 mm^2. Thus, there are 1645 and 1608 type 6 tracheae in the lantern of the two species.

Each type 6 trachea divides into 97 ± 12 (3 specimens) tracheoles for *L. terminalis* and 52 ± 6 (6 specimens) for *L. cerata*, corresponding to total numbers of $\approx 1.6 \times 10^5$ and $\approx 8.3 \times 10^4$ tracheoles. From the TXM images, we estimated the length and diameter of *L. terminalis*

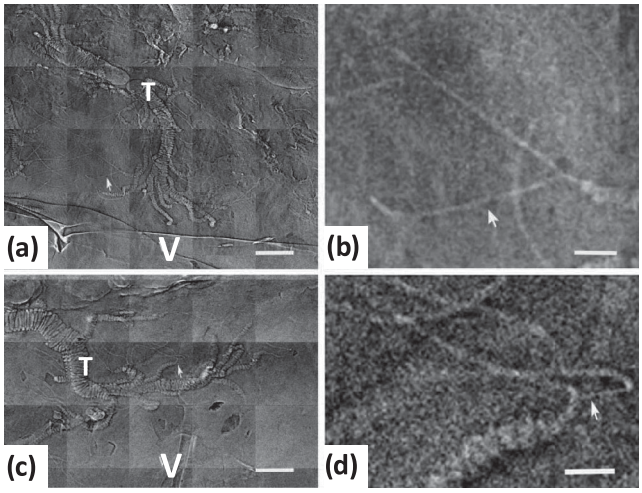

FIG. 3. TXM images of tracheoles for *L. terminalis* (a)–(b) and *L. cerata* (c)–(d). Scale bars: 10 μm [(a) and (c)], 2 μm [(b) and (d)]. Note that the tracheoles (marked by arrows) branching from type 6 tracheae (T) are always in pairs.

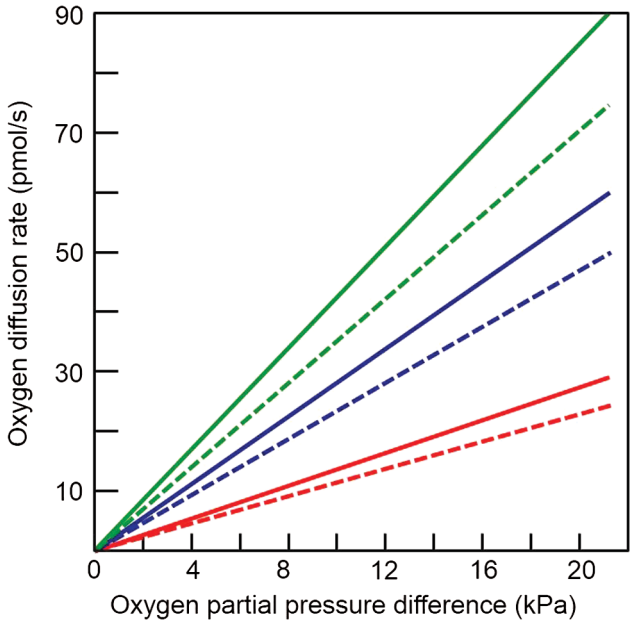

FIG. 4 (color online). Evaluated oxygen diffusion rate (p mol/s) from tracheoles to tissues. The red, blue, and green curves are for the different k_L values, $k_L = 1.0 \times 10^{-4}$, 2.0×10^{-4}, and 3.0×10^{-4} m/s. The solid and dashed lines correspond to *L. terminalis* for *L. cerata*.

tracheoles, obtaining 10 ± 1.6 μm (6 specimens) and 0.23 ± 0.01 μm (6 specimens). Thus, the surface of a tracheole is 7.4 μm^2, and the total tracheole area is $A = 1.17$ mm^2 per lantern. For *L. cerata*, the tracheole length and diameter are 12 ± 0.6 μm (6 specimens) and 0.30 ± 0.02 μm (6 specimens), and the surface area per lantern is $A = 0.97$ mm^2.

To apply Henry's law, we combined (see the Appendix) A with p and with the oxygen mass transfer coefficient k_L. Unfortunately, the exact p value is not known. Its absolute (but unrealistic) maximum is the atmospheric partial pressure, 21 kPa. According to Painmanakul *et al.* [27], k_L at 20 °C ranges from 1.0×10^{-4} to 3.0×10^{-4} m/s [15]. We thus performed calculations with three different k_L values, 1.0, 2.0, and 3.0×10^{-4} m/s.

Figure 4 shows the results. Using the extreme value $p = 21$ kPa and the largest k_L value, we obtained the above-mentioned limit diffusion rates, 88.1 and 73.4 p mol/s. However, the extreme p value makes these limit rates unrealistic. To reach more reasonable estimates, we noted that the p value between tracheoles and mitochondria in wing muscles is 5 kPa [28]. Using this value and $k_L = 3.0 \times 10^{-4}$ m/s, we obtained the realistic upper fluxes of 21 and 17.5 p mol/s for *L. terminalis* and *L. cerata*.

One fact illustrates the importance of our quantitative measurements of the total area of the smallest branches. Estimates of the oxygen diffusion from spiracles to large tracheae give much larger rates that could lead to wrong conclusions about the capacity to simultaneously accommodate flashing and mitochondria functions. For example, the diffusion rate to type 4 tracheae—evaluated from the oxygen diffusion coefficient and from the position-dependent oxygen concentration, for a p value of 1 kPa—is in the range of nmol/s. However, this is not relevant for the diffusion to photocytes, which is kept small by the tracheole area. The limited oxygen diffusion allowed by the tracheoles also excluded the presence of tracheal fluid, with or without modulation.

Note that the above diffusion rate is also consistent with the fact that pure oxygen induces continuous light emission [15,16]. The fivefold increase of the oxygen partial pressure with respect to our assumed value of 5 kPa is sufficient to overcome the mitochondrial consumption and disable the flashing control.

Finally, our study has an important byproduct: the evidence that the firefly lantern is optimized for light emission. Indeed, the oxygen diffusion rate from tracheoles is close to the bioluminescence consumption—consistent with Taylor and Weibel's symmorphosis hypothesis: biological structures meet the maximum functional requirements with minimum excess [29].

Flashing actually uses much less energy than other functions like flying, which raises the metabolic rate to ≈ 280 nmol O_2/g body/s [21,30]. Woods *et al.* measured only a 37% increase from rest to luminescence [31]. The metabolic rate at rest is 1.5–5.5 nmol O_2/g body/s [21,32]. Thus, the flashing rate is < 10 nmol O_2/g body/s, rather inexpensive in terms of energy consumption. This value matches our bioluminescence measurements: the *L. terminalis* 18.6 p mol/s consumption rate is only 2 nmol O_2/g body/s—consistent with Woods' results. Such a low consumption corresponds to a small gas exchange surface in the lantern: the tracheolar surface-area to tissue-volume ratio is < 3 mm^2/mm^3.

Overall, our study provides a coherent picture of the firefly lanterns and of their operation: they are optimized for energy-efficient flashing, which is controlled by inhibition of the mitochondria functions, most likely by NO. Several mechanism details remain to be analyzed, but our study solves the key open question.

We are grateful to Chia-Chi Chien for assisting us in the synchrotron microtomography measurements. We also thank Ting-Kuo Lee and Cyril Petibois for fruitful discussions. This work was supported by the National Science and Technology Program for Nanoscience and Nanotechnology, the Thematic Research Project of Academia Sinica, the Biomedical Nano-Imaging Core Facility at National Synchrotron Radiation Research Center (Taiwan), the Center for Biomedical Imaging (CIBM), and the Fonds National Suisse pour la Recherche Scientifique.

APPENDIX: EXPERIMENTAL AND EVALUATION DETAILS

Adult fireflies (from Taiwan Endemic Species Research Institute) were kept in a moderately humid environment with 12 h light-dark cycle at 20 °C, and fed with sugar in water. Live insects were placed in a closed chamber containing several drops of 4% osmium tetroxide for vapor smoking at room temperature, avoiding contact with liquid OsO_4. After 8–12 h, the lanterns became shiny black. Prechilling at −20 °C for 1 h was then used to prevent overheating during the x-ray exposure.

Imaging was performed at station BL01A1, National Synchrotron Radiation Research Center (NSRRC, Hsinchu). Each specimen was immobilized on a polypropylene tip and mounted on a sample holder. The photon energy was 4–30 keV with maximum intensity at ∼12 keV. The synchrotron source beam current was kept constant at 300 mA by topping up. A $CdWO_4$ scintillator placed 4–10 cm from the specimen converted x rays to visible light. Projection images were captured with an optical lens and a CCD camera (model 211, Diagnostic instruments, 1600×1200 pixels). We rotated the specimen from 0° to 180°, taking projection images every 0.18° (with an exposure time of 300 ms/image). To prevent specimen damage, a 1.1 mm silicon slab attenuated the x-ray beam, reducing the dose by a factor > 100. Projection images were computer reconstructed, obtaining cross-sectional slices with a size of 1600×1600 pixels. The slices were stacked and displayed in three dimensions with the AMIRA software (Visage Imaging).

For TXM, live fireflies were frozen at −20 °C for 1 h. The lanterns were quickly dissected and fixed in 4% paraformaldehyde and 2.5% glutaraldehyde for 2 h at room temperature. The specimens were then washed with 1x PBS, stained with 0.3% phosphotungstic acid for 3 days and soaked overnight in 20% sucrose solution. Before cryogenic sectioning, they were embedded in O.C.T. (Tissue-Tek) at −20 °C. A Leica CM 3050 cryostat yielded 30 μm sections from the dorsal to the ventral areas. Each section was attached to a Kapton slide. TXM was performed at station BL01B1 of NSRRC [33], with a photon energy of 7 keV. Each image was a patchwork of $16 \times 16\ \mu m^2$ panels, taken with an exposure time of 30 s per panel. The images were displayed with the Image Pro-Plus software (Media Cybernetics).

To evaluate the oxygen consumption for flashing, we measured the number of emitted photons following the method by Timmins for bioluminescent elaterid larva [15,16]. Live fireflies were immobilized on a black flannelette and the emission was measured in a dark room. Two silver electrodes were implanted into each lantern and connected to an integrated circuit that controlled the frequency and the current of the stimulating pulses. Each pulse duration was set to 1 ms to simulate neuron signals and the total stimulation time was 1 s. A radiometer (Model 1935-C, Power Meter) was placed above the firefly with the photon-sensitive area at 1.52 cm from the lantern. Light signals were recorded every 1 ms and the total recording time was 15 s. The peak emission wavelength of both *L. terminalis* and *L. cerata* was 560 nm.

We thus obtained the number of emitted photons per unit time, N. The maximum light-emission oxygen consumption was derived by dividing N by the reported [34] quantum yield, 0.41. From the measured bioluminescence intensities of 793 ± 99 and $468 \pm 75\ nW/cm^2$ in *L. terminalis* (3 specimens) and *L. cerata* (6 specimens), we obtained the values reported above for the maximum oxygen consumption rate.

Concerning the oxygen consumption for mitochondria functions, we note that according to Kluss the mitochondria differentiated zone extends 4 μm from the tracheolar periphery [9]. Thus, the mitochondria zone adjacent to each tracheole occupies ≈500 μm [3]. Polarographic assays show that 118 nmol of oxygen are used per minute by 1 mg of mitochondrial proteins [3]. The average protein density [35] is $1.45\ g/cm^3$. Thus, the estimated oxygen consumption is 127 and 66.3 p mol/s in *L. terminalis* and *L. cerata*, as reported above.

We now turn our attention to the evaluation of the area of the tracheal system. The number of vertically arranged tracheae per unit lantern area was counted using the AMIRA software on cross-sectional slices moving from the ventral side to the dorsal side. The overall field of view was divided into four regions. Trachea numbers were counted in each region and then averaged. We obtained the number of vertical tracheae per lantern by normalizing the result to the lantern area.

The number of tracheoles in a vertical trachea was directly counted in the TXM images. At least three tracheolar branches for each vertical trachea were examined. To obtain the number of tracheoles per vertical trachea that are active in light generation, we multiplied the result

by the estimated thickness of the photon-generating layer, 100 μm. The total number of tracheoles in a lantern was finally obtained by multiplying the number of tracheoles per vertical trachea and the total number of vertical tracheae in a lantern. The radius and length of the tracheoles were measured from TXM images. The total tracheole area was evaluated by adding the lateral and tip areas, and multiplying the result by the number of tracheoles.

Estimate of the oxygen diffusion rate from tracheoles to tissue.—The rate is $Ak_L(C' - C)$, where C' is the oxygen concentration in saturated tissue fluids and C the tissue oxygen concentration. Since $C = 0$ due to anoxia, this becomes $Ak_L C'$.

To calculate C', we note that $X = p/k$, where X is the oxygen molar fraction in tissue fluids and $k = 4.6 \times 10^4$ atm is the Henry's law constant for dissolved oxygen in water at 293 K. The water molar concentration is 55.6 M; thus, $C' = 55.6X/(1 - X) \approx 55.6X$ (X is of the order of 10^{-6} and therefore negligible in the denominator). Thus, the oxygen diffusion rate is $Ak_L 55.6p/k$. This result was used to calculate the values of Fig. 4.

Finally, this is how we estimated the oxygen flux from spiracles to type 4 tracheae. From the continuity equation, we derived [36] a simple linear equation linking the flux I and the oxygen concentration difference between type 4 tracheae and ambient:

$$I \approx G\Delta n,$$

where I is in mol/s, Δn is the oxygen concentration difference in molecules/m^3, and G is a constant, equal to 0.96×10^{-9} m^3/s and 1.02×10^{-10} m^3/s for *L. terminalis* and for *L. cerata*.

*Corresponding author.
cwli@life.nthu.edu.tw
†Corresponding author.
phhwu@sinica.edu.tw

[1] B. A. Trimmer, J. R. Aprille, D. M. Dudzinski, C. J. Lagace, S. M. Lewis, T. Michel, S. Qazi, and R. M. Zayas, Science **292**, 2486 (2001).
[2] H. Ghiradella and J. T. Schmidt, Integr. Comp. Biol. **44**, 203 (2004).
[3] J. R. Aprille, C. J. Lagace, J. Modica-Napolitano, and B. A. Trimmer, Integr. Comp. Biol. **44**, 213 (2004).
[4] D. W. Ow, J. R. De Wet, D. R. Helinski, S. H. Howell, K. V. Wood, and M. Deluca, Science **234**, 856 (1986).
[5] S. J. Gould and S. Subramani, Anal. Biochem. **175**, 5 (1988).
[6] S. T. Smale, Cold Sping Harb. Protocl., doi:10.1101/pdb.prot5421 (2010).
[7] Y. Erez, I. Presiado, R. Gepshtein, L. Pinto da Silva, J. C. G. Esteves da Silva, and D. Huppert, J. Phys. Chem. A **116**, 7452 (2012).
[8] L. Pinto da Silva, R. Simkovitch, D. Huppert, and J. C. G. Esteves da Silva, ChemPhysChem **14**, 2711 (2013).
[9] L. Pinto da Silva and J. C. G. Esteves da Silva, ChemPhysChem **13**, 2257 (2012).
[10] S. Marques and J. C. G. Esteves da Silva, IUBMB Life **61**, 6 (2009).
[11] H. Fraga, D. Fernandes, J. Novotny, R. Fontes, and J. C. G. Esteves da Silva, Chembiochem **7**, 929 (2006).
[12] B. C. Kluss, J. Morphol. **103**, 159 (1958).
[13] D. S. Smith, J. Cell Biol. **16**, 323 (1963).
[14] C. H. Hanna, T. A. Hopkins, and J. Buck, J. Ultrastruct. Res. **57**, 150 (1976).
[15] G. S. Timmins, E. J. Bechara, and H. M. Swartz, J. Exp. Biol. **203**, 2479 (2000).
[16] G. S. Timmins, F. J. Robb, C. M. Wilmot, S. K. Jackson, and H. M. Swartz, J. Exp. Biol. **204**, 2795 (2001).
[17] M. K. Peterson and J. Buck, Biol. Bull. **135**, 335 (1968).
[18] H. Ghiradella, J. Morphol. **153**, 187 (1977).
[19] H. Ghiradella, J. Morphol. **157**, 281 (1978).
[20] H. Ghiradella, J. Morphol. **177**, 145 (1983).
[21] T. Weis-Fogh, J. Exp. Biol. **41**, 229 (1964).
[22] G. Margaritondo, Y. Hwu, and J. H. Je, Riv. Nuovo Cimento Soc. Ital. Fis. **27**, 1 (2004).
[23] R. Meuli, Y. Hwu, J. H. Je, and G. Margaritondo, European radiology **14**, 1550 (2004).
[24] S. R. Wu, C. H. Lin, Y. S. Chen, Y. Y. Chen, Y. Hwu, Y. S. Chu, and G. Margaritondo, J. Phys. D **46**, 494005 (2013).
[25] C. C. Chien *et al.*, Biotechnology advances **31**, 375 (2013).
[26] T. Y. Chen, Y. T. Chen, C. L. Wang, I. M. Kempson, W. K. Lee, Y. S. Chu, Y. Hwu, and G. Margaritondo, Opt. Express **19**, 19919 (2011).
[27] P. Painmanakul, J. Wachirasak, M. Jamnongwong, and G. Hebrard, Eng. J. **13**, 13 (2009).
[28] J. N. Maina, Anat. Rec. **261**, 25 (2000).
[29] C. R. Taylor and E. R. Weibel, Respir. Physiol. **44**, 1 (1981).
[30] J. F. Harrison and S. P. Roberts, Annu. Rev. Physiol. **62**, 179 (2000).
[31] W. A. Woods, Jr., H. Hendrickson, J. Mason, and S. M. Lewis, Am. Nat. **170**, 702 (2007).
[32] R. F. Chapman, *The Insects: Structure and Function*, 4th ed. (Cambridge University Press, Cambridge, England, 1998).
[33] Y.-F. Song *et al.*, J. Synchrotron Radiat. **14**, 320 (2007).
[34] Y. Ando, K. Niwa, N. Yamada, T. Enomoto, T. Irie, H. Kubota, Y. Ohmiya, and H. Akiyama, Nat. Photonics **2**, 44 (2008).
[35] M. L. Quillin and B. W. Matthews, Acta Crystallogr. Sect. D **56**, 791 (2000).
[36] Y.-L. Tsai *et al.* (unpublished).